

Real Time Motion Planning Using Constrained Iterative Linear Quadratic Regulator for On-Road Self-Driving

Changxi You

Abstract—Collision avoidance is one of the most challenging tasks people need to consider for developing the self-driving technology. In this paper we propose a new spatiotemporal motion planning algorithm that efficiently solves a constrained nonlinear optimal control problem using the iterative linear quadratic regulator (iLQR), which takes into account the uncertain driving behaviors of the traffic vehicles and minimizes the collision risks between the self-driving vehicle (referred to as the “ego” vehicle) and the traffic vehicles such that the ego vehicle is able to maintain sufficiently large distances to all the surrounding vehicles for achieving the desired collision avoidance maneuver in traffic. To this end, we introduce the concept of the “collision polygon” for computing the minimum distances between the ego vehicle and the traffic vehicles, and provide two different solutions for designing the constraints of the motion planning problem by properly modeling the behaviors of the traffic vehicles in order to evaluate the collision risk. Finally, the iLQR motion planning algorithm is validated in multiple real-time tasks for collision avoidance using both a simulator and a level-3 autonomous driving test platform.

Keywords: iLQR, motion planning, collision avoidance, uncertainty, Gaussian integral.

I. INTRODUCTION

Self-driving technique promises to partially or completely eliminate human driver behavioral error by reasonably rectifying the driver’s inappropriate command during driving, which is expected to significantly enhance the vehicle’s driving safety and represents a major trend in the future intelligent transportation systems.

Planning is one of the most important parts for developing the self-driving vehicles, which is mainly responsible for three tasks, including mission planning, where a routing problem is solved, decision making, where the vehicle takes an appropriate action according to certain strategy, and motion planning, where the vehicle plans its future trajectory as a function of space or time [1]–[3]. In this paper we only concentrate on motion planning. There are two different kinds of motion planning solutions in literature: 1) Path planning in the spatial domain with an additional speed profile generation in the temporal domain [4], [5], where planning in space and planning in time are done sequentially in two separate steps. 2) A single solution where the trajectory is directly generated in the spatiotemporal domain, which is referred to as motion planning in this paper.

Over the past decade numerous path planning algorithms have been developed using different methodologies, which can be categorized into three groups, namely, sampling [2], [6], graph-search [7], [8], and geometry-based path planning [9]–[11]. In [2] the authors proposed a real-time path planning algorithm based on Rapidly-exploring Random Trees (RRTs), which can efficiently explore the space to handle obstacle avoidance problems. Cimurs et al.

used Dijkstra’s algorithm to find the shortest viable path by connecting the Voronoi vertices, such that the path keeps a safe distance to all the obstacles in the environment [8]. In [12] a dynamic path planning algorithm based on D^* is developed in order to avoid obstacles in complex environment involving multiple corners. All the above mentioned path planning algorithms require an additional design of the path smoother to obtain the better continuity and smoothness. The geometry-based path planning methods may provide better smoothness by using a combination of arcs [13], [14], clothoids [14], Bézier [15]–[17] and polynomials [13].

Motion planning in the spatiotemporal domain is a single solution that can simultaneously explore/exploit the spatial domain and the temporal domain for trajectory generation. Hence, it is expected to be able to satisfy the requirements for the most challenging autonomous driving tasks such as emergent collision avoidance and off-road high speed racing. Typical single-solution motion planning algorithms in the literature mainly include two categories: 1) sampling-based graph search [18]–[21] and 2) trajectory optimization by solving optimal control problems [22]–[26].

Pivtoraiko et al. defined the so called “state lattice” using a searching graph by discretizing the state space for a moving robot, where the vertices represent the kinematic state of the robot and the edges represent the feasible motions for the transitions between the neighboring states [19]. They successfully implemented both the A^* [27] and the D^* [28] search algorithms on a robot for off-road obstacles avoidance. The authors in [21] extended the state-lattice idea for autonomous driving in the structured environments, which was implemented in real-time on an autonomous passenger vehicle using a GPU. The sampling-based approaches are considered to be computationally expensive for evaluating the costs of a large number of the sampling trajectories [29]. Another direction for developing the spatiotemporal motion planning is related to the optimal control theory. Chandru et al. solved a model predictive control (MPC) problem for generating the safe lane change maneuvers in dense traffic [22]. To better satisfy the constraints of the nonlinear vehicle dynamics for motion planning, Obayashi et al. formulated a nonlinear MPC (NMPC) problem for achieving more accurate motion planning [23]. Nevertheless, the constrained NMPC is still a very hard problem to solve in general, which depends strongly on the system dynamics and the nonlinear constraints. Alternatively, an increasing number of the methods based on dynamic programming (DP) have been developed in the literature for solving the nonlinear optimization problems, such as the differential dynamic programming (DDP) [30] and the iterative linear quadratic regulator (iLQR) [24], [26], which may promise to provide better computation efficiency than NMPC. The authors in [24] proposed a constrained iLQR algorithm that efficiently solves the optimal control problem for motion

planning under nonlinear constraints, which, indeed, shows some promising results on real-time collision avoidance.

Contributions

This paper extends the iLQR motion planning algorithm from [24], focusing on improving the ability of the autonomous vehicle in the dynamically changing environments for achieving the safe driving in different challenging tasks (i.e., emergent collision avoidance). To this end, we wish to accurately determine any possible overlap between the candidate future trajectory of the ego vehicle (EV) and the predicted trajectories of the surrounding traffic vehicles (TV), such that we can further refine the planned trajectory of the EV to ensure the driving safety over the next couple of seconds.

The main contribution of this paper is summarized as follows: 1) We propose to use a “collision polygon” to evaluate the collision risk in the design of the iLQR motion planning algorithm, where the collision polygon is defined using the Minkowski sum of the bounding polygons of the self-driving vehicle and the obstacles at each predicted time step. This collision polygon can be conveniently computed and it provides a more accurate result for detecting the possible overlap between the future trajectories of the EV and the TVs than using the approximating ellipses or circles in [26], [31]. 2) Next, we propose to use two methods for designing the constraints of the motion planning problem by considering the uncertain behaviors of the surrounding TVs, which, namely, include the minimum distance regulation (MDR) where we assume the TVs’ behaviors can be exactly predicted, and the minimum risk regulation (MRR) where we assume the behaviors of the surrounding TVs are suffering from certain uncertainties. To ease the computation work, a cone zone from the collision polygon is selected for efficiently computing the minimum distance between EV and the surrounding TVs. It is worth mentioning that in the MRR formulation we assume the predicted trajectory of each TV to be a Gaussian process, and design a sampling-based algorithm to evaluate the Gaussian integral over the cone zone (collision probability) and its first order and second order partial derivatives with respect to certain parameters (gradient and Hessian). As far as the authors know, we are the first to provide the detailed iLQR formulation that is able to handle the uncertainty of the predicted trajectories of the TVs by solving the Gaussian integral. 3) Instead of computing the collision probability by solving the Gaussian integrals subject to the arbitrary linear constraints, we further refine the MRR method by computing the expected cost using a barrier function of the distance between the EV and each TV having the uncertain predicted trajectories. This modification makes the iLQR motion planning algorithm possible for real-time implementation. 4) The approach in this paper is validated using both simulations and real-world field tests. Specifically, we implemented the iLQR algorithm in more than a hundred of manually designed test cases for emergent collision avoidance, which provides solid results to show both the efficiency and the effectiveness of the iLQR algorithm for the real-time collision avoidance of the self-driving vehicle in the dynamically-changing traffic environments.

The rest of the paper is organized as follows: Section II formulates the optimal control problem we want to solve

for motion planning. Section III briefly introduces the background theory of the iLQR approach. Section IV provides the detailed design of the cost functions and the constraints for motion planning. Section V validates the iLQR motion planning algorithm in a number of testing cases using both the simulation results and the real-world experiments. Finally, Section VI summarizes the results of this study.

II. PROBLEM DESCRIPTION

Given the initial state x_{start} of the EV, motion planning is the problem one solves for the desired future trajectory of the EV starting from x_{start} to a finite time horizon by maximizing (minimizing) certain reward (cost) with respect to certain constraints from the physical world. By designing the cost functions and the constraints, one is able to achieve the optimal driving maneuvers in different tasks by solving motion planning, such as lane-switching, on/off ramp merging and collision avoidance. Mathematically, this problem can be described as follows,

$$\mathbf{x}^*, \mathbf{u}^* = \arg \min_{\mathbf{x}, \mathbf{u}} \left\{ J(\mathbf{x}, \mathbf{u}) = \ell^f(x_T) + \sum_{k=0}^{T-1} \ell(x_k, u_k) \right\}, \quad (1a)$$

$$\text{s.t.} \quad x_{k+1} = f(x_k, u_k), \quad (1b)$$

$$x_0 = x_{\text{start}}, \quad (1c)$$

$$\text{and} \quad g(x_k, u_k) < 0, \quad (1d)$$

$$g^f(x_T) < 0, \quad k = 0, 1, \dots, T-1. \quad (1e)$$

where $\mathbf{x} = \{x_k\}_{k=0, \dots, T}$ and $\mathbf{u} = \{u_k\}_{k=0, \dots, T}$ denote the state time series and the control time series, respectively; ℓ and ℓ^f represent the process cost and the terminal cost, respectively; g and g^f represent the process constraint and the terminal constraint, respectively. k denotes the time step and T denotes the total number of the steps for motion planning. The function $f(\cdot)$ in (1b) represents the dynamics equation of the vehicle.

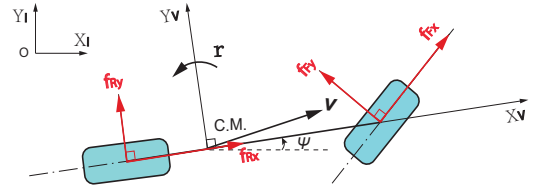


Fig. 1. Single-track vehicle model.

Fig. 1 shows the single-track vehicle dynamics model. X_I-O-Y_I and X_V-CM-Y_V denote the inertial frame and the body-fixed frame, respectively. Furthermore, v denotes the velocity at the vehicle’s center of mass (CM), and ψ and r denote the yaw angle and the yaw rate of the vehicle, respectively. The symbols f_{ij} ($i = F, R$ and $j = x, y$) denote the longitudinal and lateral friction forces at the front and rear wheels.

The computations for the tire forces f_{ij} ($i = F, R$ and $j = x, y$) are important for emergent collision avoidance, especially for the cases where the road friction conditions are poor. Nevertheless, sometimes one still have to sacrifice the vehicle modeling accuracy by ignoring the tire dynamics in order to simplify the mathematical problem to solve for the better real-time implementation speed. The feasibility of the solutions by solving such simplified

motion planning problem can be guaranteed by properly designing the constraints considering the tire dynamics and the road friction condition. Hence, we model the motion of the EV using only the kinematic equations and define the system state by $x = [p^x, p^y, v, \psi]^T$, and define the control by $u = [a, r]^T$, where (p^x, p^y) represent the coordinates of the CM of the EV in certain ground-fixed frame (i.e., $X_I - O - Y_I$), and a denotes the longitudinal acceleration. The dynamics equation $f(\cdot)$ in (1b) can be given by (2a)-(2d),

$$p_{k+1}^x = p_k^x + v_k \cos \psi \, dt, \quad (2a)$$

$$p_{k+1}^y = p_k^y + v_k \sin \psi \, dt, \quad (2b)$$

$$v_{k+1} = v_k + a_k \, dt, \quad (2c)$$

$$\psi_{k+1} = \psi_k + r_k \, dt, \quad (2d)$$

where dt is the time interval used to discretize the system.

The most popular techniques for solving the nonlinear optimal control problem in (1) may include the sequential quadratic programming (SQP) [32] and the interior-point optimizer (IPOPT) [33]. Although both the SQP and the IPOPT have shown the powerful capability for solving the nonlinear constrained optimization problems, they are initially designed for the more general-purpose optimizations where the gradients are computed using finite difference, thus making them difficult to use for the real-time motion planning. This paper adopts the iLQR to solve the motion planning problem in (1), since the iLQR is expected to be faster than both the IPOPT and the SQP [24].

III. CONSTRAINED ITERATIVE LQR

iLQR is a shooting-based method that optimizes the trajectory of the vehicle by tuning the control variables instead of directly tuning the trajectory itself. This approach is initially designed to solve the unconstrained optimization problems based on dynamic programming [31], [34]. In this section we introduce the basic theory of the iLQR and the main idea of using the iLQR to solve the constrained motion planning problem.

A. Basic Theory

Let us ignore the constraints in (1d)-(1e) for the moment and assume that we want to solve only the unconstrained optimization problem in (1a)-(1c). The iLQR then computes the optimal control strategy for the k th time step using dynamic programming following the Bellman equation,

$$V(x_k) = \min_{u_k} \left[\ell(x_k, u_k) + V(x_{k+1}) \right], \quad (3)$$

where $V(\cdot)$ is the value function that represents the minimum cost-to-go starting at the current state x_k . We then define the state-control value function Q as follows,

$$\begin{aligned} Q(x_k, u_k) &= \ell(x_k, u_k) + V(x_{k+1}), \\ &= \ell(x_k, u_k) + V(f(x_k, u_k)). \end{aligned} \quad (4)$$

In order to derive for the optimal control strategy, we need to perturb $Q(\cdot)$ around (x_k, u_k) as follows,

$$P(\delta x_k, \delta u_k) = Q(x_k + \delta x_k, u_k + \delta u_k) - Q(x_k, u_k), \quad (5)$$

where $P(\cdot)$ denotes the perturbation and $(\delta x_k, \delta u_k)$ denote the small variations in the state and the control, respectively. Next, we quadratize the perturbation function $P(\cdot)$

around $(0,0)$, which can be approximated by its second-order Taylor expansion,

$$P(\delta x_k, \delta u_k) \approx \frac{1}{2} \begin{bmatrix} 1 \\ \delta x_k \\ \delta u_k \end{bmatrix}^T \begin{bmatrix} 0 & P_x^T & P_u^T \\ P_x & P_{xx} & P_{xu} \\ P_u & P_{xu} & P_{uu} \end{bmatrix} \begin{bmatrix} 1 \\ \delta x_k \\ \delta u_k \end{bmatrix}, \quad (6)$$

where the subscripts of P denote the first and second order partial derivatives of $P(\cdot)$, which are given by

$$P_x = \frac{\partial \ell}{\partial x} \Big|_{x_k, u_k} + \frac{\partial f}{\partial x} \Big|_{x_k, u_k}^T \cdot \frac{\partial V}{\partial x} \Big|_{x_{k+1}, u_{k+1}} \triangleq \ell_x + f_x^T V'_x, \quad (7a)$$

$$P_u = \frac{\partial \ell}{\partial u} \Big|_{x_k, u_k} + \frac{\partial f}{\partial u} \Big|_{x_k, u_k}^T \cdot \frac{\partial V}{\partial x} \Big|_{x_{k+1}, u_{k+1}} \triangleq \ell_u + f_u^T V'_x, \quad (7b)$$

$$\begin{aligned} P_{xx} &= \frac{\partial^2 \ell}{\partial x^2} \Big|_{x_k, u_k} + \frac{\partial f}{\partial x} \Big|_{x_k, u_k}^T \cdot \frac{\partial^2 V}{\partial x^2} \Big|_{x_{k+1}, u_{k+1}} \cdot \frac{\partial f}{\partial x} \Big|_{x_k, u_k} \\ &\quad + \frac{\partial V}{\partial x} \Big|_{x_{k+1}, u_{k+1}} \cdot \frac{\partial^2 f}{\partial x^2} \Big|_{x_k, u_k} \triangleq \ell_{xx} + f_x^T V'_{xx} f_x + V'_x f_{xx}, \end{aligned} \quad (7c)$$

$$\begin{aligned} P_{uu} &= \frac{\partial^2 \ell}{\partial u^2} \Big|_{x_k, u_k} + \frac{\partial f}{\partial u} \Big|_{x_k, u_k}^T \cdot \frac{\partial^2 V}{\partial x^2} \Big|_{x_{k+1}, u_{k+1}} \cdot \frac{\partial f}{\partial u} \Big|_{x_k, u_k} \\ &\quad + \frac{\partial V}{\partial x} \Big|_{x_{k+1}, u_{k+1}} \cdot \frac{\partial^2 f}{\partial u^2} \Big|_{x_k, u_k} \triangleq \ell_{uu} + f_u^T V'_{xx} f_u + V'_x f_{uu}, \end{aligned} \quad (7d)$$

$$\begin{aligned} P_{xu} &= P_{ux}^T = \frac{\partial^2 \ell}{\partial x \partial u} \Big|_{x_k, u_k} + \frac{\partial f}{\partial x} \Big|_{x_k, u_k}^T \cdot \frac{\partial^2 V}{\partial x^2} \Big|_{x_{k+1}, u_{k+1}} \cdot \frac{\partial f}{\partial u} \Big|_{x_k, u_k} \\ &\quad + \frac{\partial V}{\partial x} \Big|_{x_{k+1}, u_{k+1}} \cdot \frac{\partial^2 f}{\partial x \partial u} \Big|_{x_k, u_k} \triangleq \ell_{xu} + f_x^T V'_{xx} f_u + V'_x f_{xu}. \end{aligned} \quad (7e)$$

In order to ease the computation, a common simplification for the iLQR is to eliminate the second-order terms f_{xx} , f_{xu} and f_{uu} in (7c)-(7e). Hence, the optimal control variation can be determined by minimizing $P(\delta x_k, \delta u_k)$,

$$\delta u_k^* = \arg \min_{\delta u_k} P(\delta x_k, \delta u_k). \quad (8)$$

We then let $\partial P(\delta x_k, \delta u_k) / \partial (\delta u_k) = P_u + P_{ux} \delta x + P_{uu} \delta u = 0$ and obtain the following equation,

$$\delta u_k^* = H + G \cdot \delta x_k, \quad (9)$$

where $H = -P_{uu}^{-1} P_u$ and $G = -P_{uu}^{-1} P_{ux}$. The first and second order partial derivatives of the value function $V(\cdot)$ with respect to x are given by

$$V_x = P_x - P_u P_{uu}^{-1} P_{ux}, \quad (10a)$$

$$V_{xx} = P_{xx} - P_{xu} P_{uu}^{-1} P_{ux}. \quad (10b)$$

The results in (7)-(10) indicate that if certain reference state sequence $\hat{\mathbf{x}} = \{\hat{x}_k\}_{k=0, \dots, T}$ and the corresponding control sequence $\hat{\mathbf{u}} = \{\hat{u}_k\}_{k=0, \dots, T}$ are provided, one is able to quadratize the system $f(\cdot)$ and the cost $\ell(\cdot)$ about the reference (\hat{x}_k, \hat{u}_k) from $k = T$ to $k = 0$ and compute the optimal control variations δu_k^* for each time step k using the dynamic programming method. Hence, the essential part of one single iLQR iteration contains a pair of the forward propagation and the backward propagation processes, where the forward propagation evaluates the control sequence $\hat{\mathbf{u}}$ over the planning time horizon and updates the value function $V(\cdot)$ along the planned trajectory $\hat{\mathbf{x}}$, and the backward propagation computes the control update gains H and G at each time step and slightly adjusts the control sequence $\hat{\mathbf{u}}$ by adding the optimal control variations δu^*

in order to minimize the cost-to-go $V(\cdot)$. Fig. 2 graphically shows this idea, where the black curve $\{\hat{x}_k\}_{k=0\dots T}$ represents the reference trajectory before optimization, and the red curve represents the newly generated trajectory after one single iLQR iteration. The symbol x_T in the figure denotes the target state. Such processes can be repeated for a number of iterations until certain desired trajectory is found.

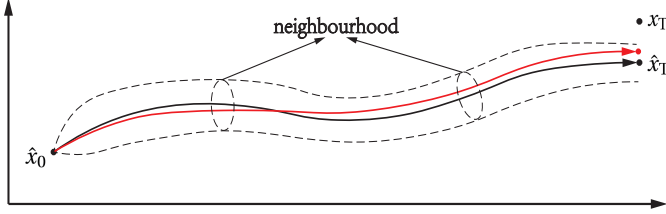


Fig. 2. iLQR trajectory optimization in a single iteration.

B. Barrier Function

We recall the fact that the constraints in (1d)-(1e) have been ignored at the beginning of Section III-A. The most popular idea to solve the constrained optimization problem in (1a)-(1e) using the iLQR is to relax the hard constraints by transforming them into a couple of the cost terms using different kinds of barrier functions, such as the exponential barrier function [26], [31] and the log barrier function [24]. This method is referred to as the constrained iLQR in the literature [24], [26], [31], [34].

In this paper we select to use the exponential barrier function instead of the log barrier function, since the log barrier function is not defined on the negative domain, which may cause the infeasibility problem during the implementation of the iLQR. Given the constraint function $g(x_k, u_k) < 0$ in (1d), for instance, the new cost term transformed using the exponential barrier function can be defined as follows,

$$b(x_k, u_k) = q_1 \exp(q_2 g(x_k, u_k)), \quad (11)$$

where $q_1 > 0$, $q_2 > 0$ are the coefficients to be designed. Furthermore, equation (11) can be quadratized as follows,

$$b(x_k + \delta x_k, u_k + \delta u_k) \approx b(x_k, u_k) + \frac{1}{2} \begin{bmatrix} 1 \\ \delta x_k \\ \delta u_k \end{bmatrix}^T \begin{bmatrix} 0 & b_x^T & b_u^T \\ b_x & b_{xx} & b_{xu} \\ b_u & b_{ux} & b_{uu} \end{bmatrix} \begin{bmatrix} 1 \\ \delta x_k \\ \delta u_k \end{bmatrix}, \quad (12)$$

where

$$b_x = q_1 q_2 \exp(q_2 g(x_k, u_k)) g_x, \quad (13a)$$

$$b_u = q_1 q_2 \exp(q_2 g(x_k, u_k)) g_u, \quad (13b)$$

$$b_{xx} = q_1 q_2 \exp(q_2 g(x_k, u_k)) (q_2 g_x g_x^T + g_{xx}), \quad (13c)$$

$$b_{uu} = q_1 q_2 \exp(q_2 g(x_k, u_k)) (q_2 g_u g_u^T + g_{uu}), \quad (13d)$$

$$b_{xu} = q_1 q_2 \exp(q_2 g(x_k, u_k)) (q_2 g_x g_u^T + g_{xu}), \quad (13e)$$

and where the subscripts of $g(\cdot)$ represent the first order and the second order partial derivatives of the constraint function. The equations in (13a)-(13e) provide the results for the gradients and the Hessian matrices of the trans-

formed cost function in (11). More results and discussions on the constrained iLQR can be found in [31].

IV. MOTION PLANNING

In this section we design the cost functions and the constraints for the motion planning problem in (1a)-(2d). Specifically, we provide two different solutions for collision avoidance: 1) The state estimations and the predicted trajectories for the TVs are provided in high confidence. In this case one is able to trust the quality of the predicted trajectories and further ensure the driving safety by maintaining the distances between the EV and the TVs to be larger than certain safe distance since the distances between the EV and the TVs can be exactly computed. 2) The state estimations and the predicted trajectories for the TVs are provided with considerable uncertainties. Instead of directly maintaining the distances between the EV and the TVs, in this case we penalize the collision probabilities between the EV and the TVs for the enhanced driving safety.

In order to simplify the mathematical expressions for the remaining part of this section, we use I_n and $O_{a \times b}$ to represent the identity matrices and the zero matrices, respectively, where n , a and b denote the dimensions for the identity matrices and the zero matrices, respectively. We first introduce the design of the cost function.

A. Cost Function

We recall the fact that the optimal control variations δu^* in (9) are computed using the gradients and the Hessian matrices of the cost function ℓ . Hence, it is convenient to design ℓ in the form of the sum of a series of quadratic expressions to ease the computation.

1) *Control Cost*: The control cost is designed to reduce the control energy that is required for achieving the target trajectory. Moreover, one can also minimize the deviation of the control signal from its desired value for providing the better smoothness of the trajectory in both the longitudinal and the lateral directions. We design the control cost as follows,

$$\ell_u = \frac{1}{2} u_k^T \begin{bmatrix} w_a & 0 \\ 0 & w_r \end{bmatrix} u_k, \quad (14)$$

where w_a and w_r are the weights to be specified.

2) *Adjusting Cost*: Next, we introduce the adjusting cost. Given the reference trajectory $\hat{\mathbf{x}} \triangleq \{\hat{x}_k\}_{k=0\dots T}$ (see Fig. 2) in each iLQR iteration, where $\hat{\mathbf{x}}$ can be obtained from the previous iteration, one may want to optimize the trajectory by gradually adjusting $\hat{\mathbf{x}}$ within its certain neighborhood such that the new trajectory cannot be obviously changed from the reference $\hat{\mathbf{x}}$ in one iteration. Such designed cost is referred to as the ‘‘adjusting cost’’ in this work, which is used to mitigate the dynamic effect of the modeling errors by the system linearizations about different references $\hat{\mathbf{x}}$ in different iterations. The adjusting cost is given by

$$\ell_{\hat{\mathbf{x}}} = \frac{1}{2} (x_k - \hat{x}_k)^T \begin{bmatrix} w_{p^x} & 0 & 0 & 0 \\ 0 & w_{p^y} & 0 & 0 \\ 0 & 0 & w_v & 0 \\ 0 & 0 & 0 & w_\psi \end{bmatrix} (x_k - \hat{x}_k), \quad (15)$$

where w_{p^x} , w_{p^y} , w_v and w_ψ are the weights to be specified.

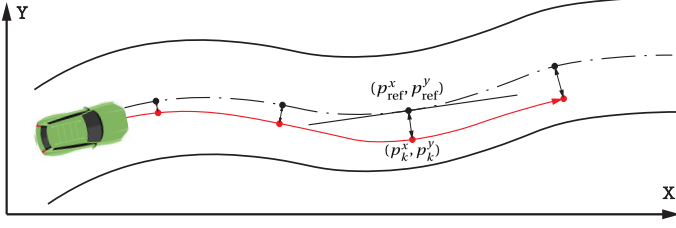


Fig. 3. Tracking error for lane keeping.

3) *Tracking Cost* : Tracking cost is usually designed for achieving better lane-keeping. To this end, for each point (p_k^x, p_k^y) we first find its reference point $(p_{\text{ref}}^x, p_{\text{ref}}^y)$, which is the closest point to (p_k^x, p_k^y) on the reference line (i.e., road center-line in Fig. 3). Moreover, one can also specify the desired speed v_{ref} accordingly. Then, the tracking cost can be determined as follows,

$$\ell_{\text{ref}} = \frac{1}{2} (Cx_k - x_{\text{ref}})^T \begin{bmatrix} w_{\text{pref}} & 0 & 0 \\ 0 & w_{\text{pref}} & 0 \\ 0 & 0 & w_{\text{vref}} \end{bmatrix} (Cx_k - x_{\text{ref}}), \quad (16)$$

where w_{pref} and w_{vref} are the weights to be specified, $x_{\text{ref}} = [p_{\text{ref}}^x, p_{\text{ref}}^y, v_{\text{ref}}]^T$, and the matrix $C = [I_3 \mid \mathbf{0}_{3 \times 1}]$.

4) *Terminal Cost*: Similar with the design of the tracking cost in (16), we design the terminal cost to achieve the desired orientation ψ^f and the desired speed v^f at $t = T$, which can be given by

$$\ell^f = \frac{1}{2} (C^f x_T - x^f)^T \begin{bmatrix} w_{\psi}^f & 0 \\ 0 & w_v^f \end{bmatrix} (C^f x_T - x^f), \quad (17)$$

where w_{ψ}^f and w_v^f are the weights to be specified, $x^f = [\psi^f, v^f]^T$, and the matrix $C^f = [\mathbf{0}_{2 \times 2} \mid I_2]$.

B. Constraint Function

In this section we define the constraints for motion planning. The constraint functions are used to describe certain feasible space in which the vehicle is allowed to drive, which are designed mainly by considering the safety reasons and other restrictions from the physical world.

1) *Control Constraint*: The constraints on control are represented by the following expression,

$$\begin{bmatrix} a_{\min} \\ r_{\min} \end{bmatrix} < u_k < \begin{bmatrix} a_{\max} \\ r_{\max} \end{bmatrix} \quad (18)$$

where a_{\min} and r_{\min} denote the minimum acceleration and the minimum yaw rate, respectively; a_{\max} and r_{\max} denote the maximum acceleration and the maximum yaw rate, respectively. The symbol “<” represents component-wise inequalities. The lower and upper bounds for u_k need to be carefully designed using certain reasonable values to guarantee the feasibility of such trajectory for tracking control in the next step. We denote the peak road friction coefficient as $\hat{\mu}$. Then, the following inequalities must hold,

$$-\hat{\mu}g < a_{\min} < a_{\max} < \hat{\mu}g, \quad (19a)$$

$$-\sqrt{\hat{\mu}^2 g^2 - \bar{a}^2} / C_v x_k < r_{\min} < r_{\max} < \sqrt{\hat{\mu}^2 g^2 - \bar{a}^2} / C_v x_k, \quad (19b)$$

where $\bar{a} = \max\{|a_{\min}|, |a_{\max}|\}$, $C_v = [0, 0, 1, 0]$, and $g = 9.81 \text{ [m/s}^2\text{]}$ is the gravitational acceleration constant.

2) *Boundary Constraint*: The tracking cost in (16) penalizes the deviation of the planned future trajectory from the lane center-line. Nevertheless, one still needs to consider the road boundary constraints for motion planning in order to avoid possible severe collisions with the static barriers along the boundaries. One convenient way to define these boundary constraints is to represent the boundary curves using certain order polynomial function in an appropriate frame (see Fig. 3). The boundary constraints can be described as follows,

$$C_y x_k - \Gamma_{\text{left}}(C_x x_k) < 0, \quad (20a)$$

$$C_y x_k - \Gamma_{\text{right}}(C_x x_k) > 0, \quad (20b)$$

where $C_x = [1, 0, 0, 0]$, $C_y = [0, 1, 0, 0]$, and $\Gamma_{\text{left}}(\cdot)$ and $\Gamma_{\text{right}}(\cdot)$ represent the left and right boundary curves, respectively, which are given by

$$\Gamma_{\text{left}}(x) = \sum_{k=0}^{n_1} a_k x^k, \quad \Gamma_{\text{right}}(x) = \sum_{k=0}^{n_2} b_k x^k, \quad (21)$$

where n_1 and n_2 are positive integers, and a_k and b_k are the coefficients.

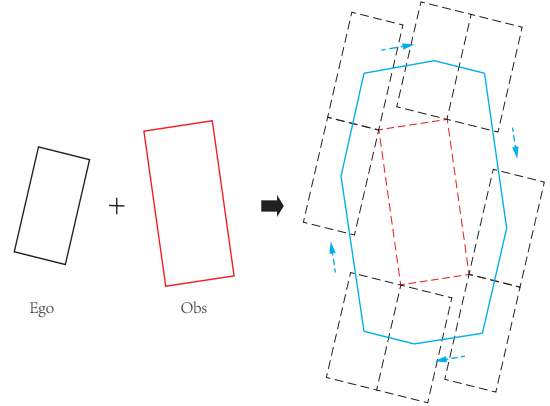


Fig. 4. Minkowski sum of the bounding polygons of EV and a TV.

3) *Obstacle Constraint*: The design of the obstacle constraints is the most important task for motion planning using iLQR, which dynamically evaluate the potential collision risk between EV and the surrounding TVs and rectify therefore the EV's future trajectory planning by decreasing the collision risk. We assume that the trajectories of the TVs are predicted with different levels of uncertainties and provide two different solutions accordingly.

Let us assume there are M surrounding TVs to be considered and define the TV set $\mathcal{S} \triangleq \{\text{TV}_j | j = 1, \dots, M\}$. Then, we represent each TV_j in \mathcal{S} using a bounding polygon in the two-dimensional space, where the bounding polygon is the convex hull of TV_j defined using a number of vertices V_1, \dots, V_L ,

$$\mathcal{B}_j \triangleq \left\{ \sum_{i=0}^L \rho_i V_i \mid V_i \in \mathbb{R}^2, \rho_i \geq 0, \sum_{i=0}^L \rho_i = 1 \right\}, \quad j = 1, \dots, M. \quad (22)$$

For the sake of simplicity we let $L = 4$ and use the bounding rectangles to approximately represent the TVs. Then, the collision polygon for TV_j can be defined using the convo-

lution of the oriented bounding rectangle of the EV and the oriented bounding rectangle of TV_j as follows (see Fig. 4),

$$\mathcal{C}_j \triangleq \{P' + P'' - P \mid P' \in \mathcal{B}, P'' \in \mathcal{B}_j\}, \quad j = 1, \dots, M, \quad (23)$$

where P and \mathcal{B} denote the centroid and the bounding rectangle of the EV, respectively. The boundary of \mathcal{C}_j can be viewed as the trace of the EV's centroid when the EV moves around the border of \mathcal{B}_j . We further represent the predicted trajectory for TV_j as

$$\mathcal{X}_j \triangleq \{\zeta_j^k \in \mathbb{R}^2 \mid k = 0, \dots, T\}, \quad (24)$$

where ζ_j^k denotes the position of the centroid for TV_j at the k th prediction time step.

Next, we design the constraints for obstacle avoidance based on the collision polygons \mathcal{C}_j using two different approaches, namely, minimum distance regulation (MDR) and minimum risk regulation (MRR).

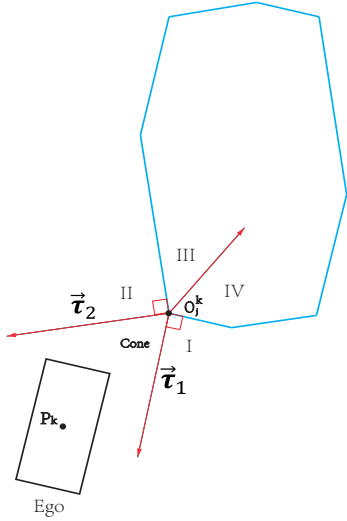


Fig. 5. Distance between EV and TV_j at the k th prediction time step.

a) *MDR*. If the prediction trajectory for TV_j can be provided with sufficient accuracy, one just needs to determine the distance d_j^k between the EV and TV_j for each predicted time step k and maintain d_j^k to be larger than certain reasonable value in order to ensure the driving safety.

We denote the collision polygon of TV_j at the time step k as \mathcal{C}_j^k . Then, we determine the closest vertex of the collision polygon \mathcal{C}_j^k to the EV's centroid P_k , which is indicated by the point O_j^k in Fig. 5. Next, we divide the two dimensional space around O_j^k into five zones, including the zone I, II, III, IV and a cone zone, where the zone III and zone IV are divided by the bisector of the angle $\angle O_j^k$. The minimum distance between the EV and the TV_j at the time step k can be computed as follows,

$$d_j^k(x_k, O_j^k) = \begin{cases} \vec{\tau}_1 \cdot \overrightarrow{O_j^k P_k}, & P_k \in \text{I} \cup \text{IV}, \\ \vec{\tau}_2 \cdot \overrightarrow{O_j^k P_k}, & P_k \in \text{II} \cup \text{III}, \\ \|\overrightarrow{O_j^k P_k}\|, & P_k \in \text{Cone}, \end{cases} \quad (25)$$

where $\vec{\tau}_1$ and $\vec{\tau}_2$ are the two normal vectors perpendicular

to the two edges of $\angle O_j^k$, respectively; P_k denotes the centroid of the EV. Furthermore, the obstacle constraints can be given by

$$d_j^k(x_k, O_j^k) - \underline{d} > 0, \quad j = 1, \dots, M, \quad (26)$$

where $\underline{d} > 0$ is the minimum required distance between EV and the TVs.

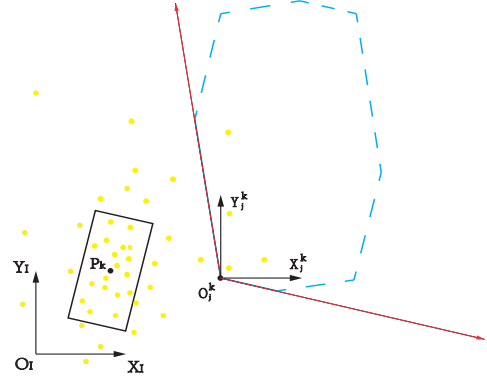


Fig. 6. The collision probability of EV and TV_j at the k th prediction time step.

b) *MRR*. The constraints in (26) are only valid when the uncertainties associated with both the state estimations and the trajectory predictions for the TVs can be neglected, but in practice this condition cannot be always satisfied. In the cases where the TVs' states are poorly measured or their future trajectories are predicted with significant uncertainties, one still needs to take into account these uncertainties for safe motion planning.

We assume the orientation of each TV is in parallel with the tangential direction of its predicted trajectory over the prediction horizon. Thus, the variance of the orientation of each TV is considered to be very low and hence negligible [35]. Consequently, we only consider the covariance of the position vector for each TV in order to model the uncertainties for the TVs' behaviors. We further neglect the covariance of the EV's position vector based on the fact that the state of the EV can be measured more accurately than the surrounding TVs.

Instead of computing the distance from the centroid of the EV P_k to the collision polygon \mathcal{C}_j^k using (25), one needs to compute the probability of P_k to be in \mathcal{C}_j^k since the position of O_j^k is no longer deterministic (see Fig. 5). Furthermore, in order to simplify the derivations, we suggest to use the cone formed by $\angle O_j^k$ instead of using the polygon \mathcal{C}_j^k itself to approximately calculate the collision probability as shown in Fig. 6. To avoid the ambiguities in the notations, in the remaining part we use " \angle " to denote a cone and use " \angle " to denote an angle, respectively.

Let us assume $O_j^k \sim \mathcal{N}(\mu_j^k, \Sigma_j^k)$ and define a new random vector $\tilde{P}_k \triangleq \overrightarrow{O_j^k P_k} = C_P x_k - O_j^k$, where $C_P = [I_2 \mid O_{2 \times 2}]$. It is not hard to figure out $\tilde{P}_k \sim \mathcal{N}(C_P x_k - \mu_j^k, \Sigma_j^k)$. Then, we just need to compute the probability of the random point \tilde{P}_k observed in the frame $X_j^k - O_j^k - Y_j^k$ (see Fig. 6) to be in

the cone $\angle O_j^k$, which can be given as follows,

$$\mathbb{P}(\tilde{P}_k \in \angle O_j^k) = \int_{\angle O_j^k} \frac{1}{2\pi \sqrt{|\Sigma_j^k|}} \exp\left(-\frac{1}{2}(\xi - \mu_j^k + C_P x_k)^T (\Sigma_j^k)^{-1} (\xi - \mu_j^k + C_P x_k)\right) d\xi, \quad (27)$$

where $|\cdot|$ represents the determinant of the matrix. We further provide the first and second order partial derivatives of the collision probability with respect to the centroid of the EV using the Leibniz integral rule, which are given by

$$\frac{\partial \mathbb{P}(\tilde{P}_k \in \angle O_j^k)}{\partial x_k} = \int_{\angle O_j^k} \mathcal{N}(\xi; C_P x_k - \mu_j^k, \Sigma_j^k) C_P^T (\xi + \mu_j^k - C_P x_k)^T (\Sigma_j^k)^{-1} d\xi, \quad (28a)$$

$$\frac{\partial^2 \mathbb{P}(\tilde{P}_k \in \angle O_j^k)}{\partial (x_k)^2} = \int_{\angle O_j^k} \mathcal{N}(\xi; C_P x_k - \mu_j^k, \Sigma_j^k) C_P^T \left((\Sigma_j^k)^{-1} (\xi + \mu_j^k - C_P x_k) (\xi + \mu_j^k - C_P x_k)^T (\Sigma_j^k)^{-1} - (\Sigma_j^k)^{-1} \right) C_P d\xi. \quad (28b)$$

Finally, the obstacle constraints that takes into account the collision probabilities can be given by (26) together with the following inequalities

$$\mathbb{P}(\tilde{P}_k \in \angle O_j^k) - \bar{\mathbb{P}} < 0, \quad j = 1, \dots, M, \quad (29)$$

where $\bar{\mathbb{P}} > 0$ is the maximum allowed collision probability between EV and the TVs.

Equations (27)-(28) provide all the necessary results that are required for minimizing the collision probability using the gradient-based optimization methods. Nevertheless, the integrals in (27)-(28) are subject to the arbitrary linear constraints and there exist no analytical solutions for them. Thus, one may have to approximate these Gaussian integrals using the numerical sampling methods [36], which may be too computationally expensive for real-time implementation.

In order to address this issue, we, alternatively, propose another approach to handle the uncertainties by using the barrier functions introduced in Section III-B. Given the TVs having the uncertain positions, the idea is that we can view the distances between the TVs and the EV as the new random variables and penalize the expected costs that are represented as the barrier functions of the random distances between the EV and the TVs, instead of penalizing their collision probabilities that are difficult to compute. To this end, we represent the constraints in (26) as the following cost terms,

$$b(\tilde{P}_k) = q_1 \exp\left(q_2(d - d_j^k(\tilde{P}_k, \mu_j^k))\right), \quad j = 1, \dots, M, \quad (30)$$

where $\tilde{P}_k \sim \mathcal{N}(C_P x_k - \mu_j^k, \Sigma_j^k)$. One should notice that we have changed the arguments of $d_j^k(\cdot)$ in order to explicitly show the dependency of (30) on the random variable \tilde{P}_k . We then penalize the expected values of the barrier functions in (30), which can be computed using the following equation,

$$\mathbb{E}[b(\tilde{P}_k)] = \int \mathcal{N}(\xi; C_P x_k - \mu_j^k, \Sigma_j^k) b(\xi) d\xi. \quad (31)$$

Furthermore, we provide the expressions for computing the

gradient and Hessian of (31) as follows,

$$\frac{\partial b(\tilde{P}_k)}{\partial x_k} = \mathbb{E}\left[b(\tilde{P}_k) C_P^T (\tilde{P}_k + \mu_j^k - C_P x_k)^T (\Sigma_j^k)^{-1}\right], \quad (32a)$$

$$\frac{\partial^2 \mathbb{E}[b(\tilde{P}_k)]}{\partial (x_k)^2} = \mathbb{E}\left[b(\tilde{P}_k) C_P^T \left((\Sigma_j^k)^{-1} (\tilde{P}_k + \mu_j^k - C_P x_k) (\tilde{P}_k + \mu_j^k - C_P x_k)^T (\Sigma_j^k)^{-1} - (\Sigma_j^k)^{-1} \right) C_P\right]. \quad (32b)$$

The equations in (31)-(32b) can be conveniently evaluated using, for instance, the unscented transform (UT) or the extended Kalman filter (EKF) technique, since we successfully get rid of the linear constraints in the Gaussian integrals (one can see (27)-(28) in contrast), which makes it possible for real-time implementation.

Algorithm 1 ILQR Motion Planning

Input: $\mathbf{x}_0, \mathbf{u}_0, \lambda_0, \lambda_{\max}, s, T, N$

Output: $\mathbf{x}^*, \mathbf{u}^*$

- 1: $\lambda \leftarrow \lambda_0$;
 - 2: $\mathbf{x}^- \leftarrow \mathbf{x}_0, \mathbf{u}^- \leftarrow \mathbf{u}_0$;
 - 3: Convert constraints (18)-(31) to costs using barrier function (11);
 - 4: $J^-, \{(f_x)_k, (f_u)_k, (\ell_x)_k, (\ell_u)_k, (\ell_{xx})_k, (\ell_{xu})_k, (\ell_{uu})_k\}_{k=0, \dots, T} \leftarrow$ forward pass using control sequence \mathbf{u}_0 ;
 - 5: Convergence \leftarrow **False**;
 - 6: **for** $i \leftarrow 0$ to N **do**
 - 7: $\{H_k, G_k\}_{k=0, \dots, T} \leftarrow$ backward pass following (3)-(10) and (33);
 - 8: $J^+, \mathbf{x}^+, \mathbf{u}^+, \{(f_x)_k, (f_u)_k, (\ell_x)_k, (\ell_u)_k, (\ell_{xx})_k, (\ell_{xu})_k, (\ell_{uu})_k\}_{k=0, \dots, T} \leftarrow$ forward pass using $\{H_k, G_k\}_{k=0, \dots, T}$;
 - 9: **if** $J^+ < J^-$ **then**
 - 10: $\lambda \leftarrow \lambda/s$;
 - 11: $J^- \leftarrow J^+$;
 - 12: $\mathbf{x}^- \leftarrow \mathbf{x}^+, \mathbf{u}^- \leftarrow \mathbf{u}^+$;
 - 13: **if** Convergence **then**
 - 14: **break**;
 - 15: **else**
 - 16: $\lambda \leftarrow s\lambda$;
 - 17: **if** $\lambda > \lambda_{\max}$ **then**
 - 18: **break**;
 - 19: **return** $\mathbf{x}^* \leftarrow \mathbf{x}^-, \mathbf{u}^* \leftarrow \mathbf{u}^-$;
-

C. Levenberg-Marquadt

It is worth mentioning that the quadratic approximations in (6) and (12) cannot guarantee the Hessian matrices (i.e., P_{xx}, P_{uu}) to be positive-definite all the time, which depends on the nonlinear dynamics of the system in (2a)-(2d) and the nonlinear cost functions in (14)-(32) for a specific motion planning problem. Nevertheless, the optimal control law computed by (9) requires the positive definiteness of P_{uu} at each time step during an iLQR iteration. To fix this issue, one could use a Levenberg-Marquadt method [34], an adaptive shift scheme [37], or simply fix the Hessian to be identity.

This paper uses the well-known Levenberg-Marquadt method to fix the Hessian and search for the optimal trajectory iteratively by appropriately adjusting the so called damping factor. The inverse matrix of the Hessian P_{uu} is computed as follows: 1) We first decompose the Hessian $P_{uu} = U\Lambda U^T$ since P_{uu} is symmetric, where $U^T U = \mathbf{I}$ are the normalized eigenvectors and Λ is the diagonal matrix of

the eigenvalues. 2) Next, we set all the negative eigenvalues in Λ to 0; 3) The inverse matrix of P_{uu} in (10) is given by

$$P_{uu}^{-1} = U(\Lambda + \lambda I)^{-1} U^T, \quad (33)$$

where $\lambda > 0$ is the damping factor. We then summarize the iLQR motion planning algorithm in Algorithm 1 (see Table I for the unknown parameters).

V. RESULTS

In this section we implement Algorithm 1 for emergent collision avoidance in different scenarios in simulation. Furthermore, we validate the motion planning algorithm in multiple real-time tasks using both a simulator and a level-3 autonomous driving test platform developed by the Tencent Autonomous Driving team, which, for short, are referred to as TadSim and TadAuto, respectively.

Since the existing work in the literature has provided sufficient comparison results between iLQR and the standard baseline motion planning algorithms (i.e., SQP) [24], which shows the great advantage of iLQR in the computation efficiency by saving 98% running time than the SQP per iteration, this paper does not repeat such comparison work as this is already done well. We, instead, concentrate on validating the iLQR algorithm in the more challenging and more complicated tasks that were not investigated enough in the existing work, such as the real-time emergent collision avoidance in the real-world dynamically-changing and uncertain traffic.

A. Simulation

First, we simulate the behaviors of several environmental TVs in Python 3.7 and implement Algorithm 1 with the MDR formulation for collision avoidance. The planning horizon for the EV at each time step is set to $\mathcal{T} = 5$ seconds, during which the predicted trajectories of the surrounding TVs are assumed to be exactly given. The time interval for the motion planning of the EV is $dt = 0.25$ seconds. Other related design parameters for the iLQR algorithm are summarized in Table I.

TABLE I
iLQR DESIGN PARAMETERS & SIMULATION CONDITION.

\mathcal{T} [sec]	5.0	planning horizon		N [-]	20	max iteration Num.					
dt [sec]	0.25	time interval		s [-]	5e2	scale					
λ_0 [-]	1.0	initial damping		λ_{\max} [-]	1e10	max damping					
a_{\max} [m/sec ²]	2.0	max acceleration		a_{\min} [m/sec ²]	-4.0	min acceleration					
r_{\max} [rad/sec]	0.25	max yaw rate		r_{\min} [rad/sec]	-0.25	min yaw rate					
d [m]	1.0	min EV/TV distance		\mathbb{P} [-]	0.1	max collision risk					
w_a	1e3	w_r	1e5	w_{p^x}	1	w_{p^y}	1	w_v	1e4	w_ψ	1e4
$w_{p^{\text{ref}}}$	1e5	$w_{v^{\text{ref}}}$	1e3	$w_{\psi^{\text{ref}}}$	1e4	w_v^{ref}	1e3	q_1	1e2	q_2	10
speed [m/s]	20.0	lat. distance [m]	-	long. distance [m]	-	length [m]	5.0	width [m]	2.0	task	-
EV	20.0	-	-	-	-	5.0	5.0	2.0	2.0	lane-keeping	-
TV ₁	10.0	-2.0	-	15.0	-	5.0	5.0	2.0	2.0	switch to left	-
TV ₂	10.0	4.0	-	0.0	-	5.0	5.0	2.0	2.0	lane-keeping	-
TV ₃	12.0	-4.0	-	-10.0	-	5.0	5.0	2.0	2.0	lane-keeping	-

We first consider a typical emergent cut-in scenario where a low speed TV suddenly switches to the lane of the EV using about 2 seconds from a neighbour lane. One can find the simulation conditions for the EV and TV₁ from Table I in this case. Since we assume the minimum acceleration of the EV to be $a_{\min} = -4.0$ [m/sec²], the minimum safe distance between EV and TV₁ should be at least $(V_{EV} - V_{TV_1})^2 / 2|a_{\min}| + (l_{EV} + l_{TV_1}) / 2 = 17.5$ [m] (larger than

15 [m]), where V_{EV} , V_{TV_1} , l_{EV} and l_{TV_1} are the initial speeds and the vehicle lengths of the EV and TV₁, respectively. This result indicates that the EV cannot avoid collision with TV₁ by braking merely without proper lateral motion. Fig. 7 plots the planned trajectory of the EV and the predicted trajectory of TV₁ over \mathcal{T} at different time instants, where the symbols v , a , and r denote the velocity [m/s], the acceleration [m/s²] and the yaw rate [rad/s] of the EV, respectively. The result shows that the EV is able to avoid the collision with TV₁ by temporally taking up the left neighbour lane which is available when TV₁ is changing the lane.

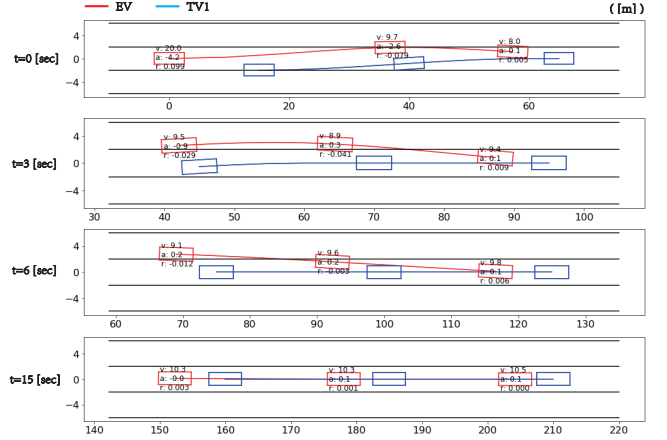


Fig. 7. Collision avoidance in a 3-lane scenario with single TV.

Next, we make the collision avoidance task more challenging by including more TVs into the driving scenario (see TV₂ and TV₃ in Table I), such that both the left lane and the right lane of the EV will be occupied when the cut-in behavior of TV₁ takes place. The new simulation trajectories are plotted in Fig. 8.

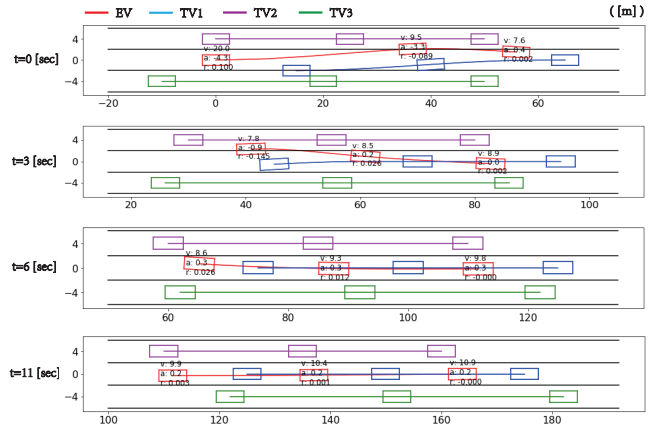


Fig. 8. Collision avoidance in a 3-lane scenario with multiple TVs.

The result in Fig. 8 shows that the EV is able to avoid collision with both TV₁ and TV₂ by more reasonably using the space of its current lane and the space of the left neighbour lane. By comparing the results in Fig. 7 and Fig. 8 one can see that in the first case half of the left lane was occupied by the EV for collision avoidance, while in the second case only a quarter of the left lane or so was occupied such that the EV is able to keep certain safe distance from TV₂ at the same time.

Furthermore, we repeat the two tasks above in Fig. 7 and Fig. 8 by implementing Algorithm 1 with the MRR formulation, respectively, while assuming each point of the predicted trajectories of the TVs to be suffering from the uniform covariance $\Sigma_j^k = 0.25 \times I_2$. The simulation results are shown in Fig. 9. By comparing Fig. 9 (a) and Fig. 9 (b)

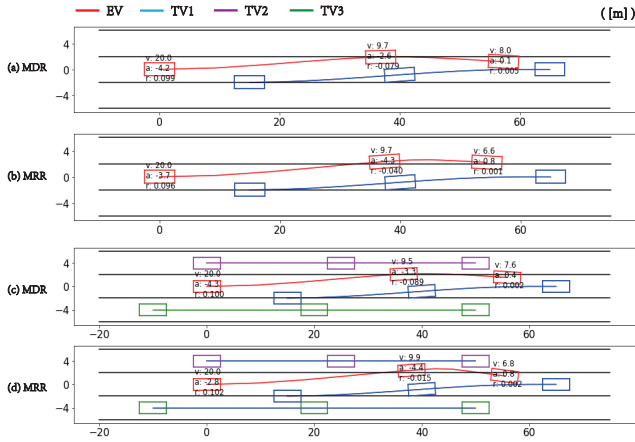


Fig. 9. Comparison between MDR & MRR in both cases.

one sees that the planned trajectory for the EV using the MRR formulation shows more bending in the middle of the trajectory, since we assume the position of TV_1 is not exactly predicted and a larger distance between the two vehicles is required for better the safety. By comparing Fig. 9 (b) and Fig. 9 (d) one sees that the planned trajectory for the EV shows more bending at the end of the trajectory in order to avoid the collision with TV_2 on the left, whose position is also not exactly predicted by assumption. This result shows the effectiveness of the MRR method to handle the environmental obstacles' uncertainties for collision avoidance. Nonetheless, the EV has to keep a larger distance from the surrounding TVs in the uncertain traffic environment, which looks quite conservative and the smoothness of the EV's trajectory also gets worse. Hence, it is still important to enhance the environmental perception ability of the self-driving vehicles and further improve the trajectory prediction quality for the TVs to minimize the effect of the uncertainties for the better self-driving performance.

B. Real-Time Implementation

Next, we implement the motion planning algorithm in real-time using TadSim and TadAuto, respectively. TadSim is a real-time traffic simulation platform that is built for developing the self-driving technology, where the self-driving vehicle is modeled with 27 degrees of freedom and the traffic vehicles are mainly controlled by the intelligent driver model [38]. TadSim is especially suitable for generating the diverse high-fidelity vehicle maneuvers in all kinds of driving scenarios. Fig. 10 shows the interface of TadSim, which includes an EV in the middle and multiple TVs driving on a high-definition map. We manually design more than a hundred of testing cases by mimicking the various cut-in maneuvers of the TVs using TadSim, and implement the iLQR motion planning algorithm for collision avoidance in all testing cases. The algorithm is coded in C++ 11 to obtain the better implementation speed.

TABLE II
SIMULATION RESULT WITH/WITHOUT iLQR.

	Ave. acceleration [m/s ²]	Ave. jerk [m/s ³]	Accident rate
Braking-only	-1.32	1.25	14/121
iLQR	-0.25	0.84	0/121
Improvement	81.1%	32.8%	-

Table II summarizes the simulation results. The item “braking-only” corresponds to the experiments where only the longitudinal control (i.e., intelligent driver model) is applied for collision avoidance during lane-keeping. One sees that the iLQR motion planning algorithm is able to safely pass all the testing cases without any collision, while providing the better driving comfort by obviously improving the average acceleration and the average jerk.

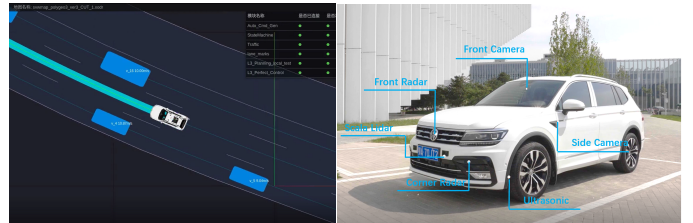


Fig. 10. Simulation interface of TadSim (left) and TadAuto (right).

Furthermore, we implement the iLQR motion planning algorithm on the TadAuto platform in the real-world traffic environment, where TadAuto is a level-3 autonomous vehicle which is mainly equipped with five radars and a front-view camera. The real-world field experiments show similar results with the simulations using TadSim (see Fig. 10). We demonstrate the collision avoidance behavior of the self-driving vehicle using the video which can be found via the link below ¹. We do not provide more results due to the limit of space.

VI. CONCLUSION

We propose a new iLQR motion planning algorithm for developing the self-driving technology, which concentrates on handling the uncertain behaviors of the TVs in the traffic for emergent collision avoidance during lane-keeping. This approach can be easily extended for more driving scenarios such as lane-changing and on/off ramp merging by adjusting a little bit the design of the cost functions.

We use the so-called “collision polygon” to determine the minimum distance between the EV and each TV of interest in the traffic, and introduce two different methods for designing the constraints of the motion planning problem to handle the uncertain behaviors of the surrounding TVs. The iLQR motion planning algorithm is further validated using both the simulation results and the real-word experiments for collision avoidance in traffic. Promising results are observed which show both the implementation efficiency and the effectiveness of the iLQR motion planning algorithm in multiple manually designed driving experiments, while improving obviously the driving comfort simultaneously.

Future work will focus on improving the work to incorporate special obstacles such as the pedestrians that

¹The videos are available on the youtube channel: <https://youtu.be/BhR98UpTDEg>

may need extra attention for motion planning. Also more experiments and test cases considering different levels of the uncertainties in the state estimations for the obstacles will be designed for further possible improvement of the driving safety.

ACKNOWLEDGMENT

The authors would like to thank the Tencent autonomous driving team for providing the necessary assistance for conducting the experiments.

REFERENCES

- [1] S. Brechtel, T. Gindele, and R. Dillmann, "Probabilistic MDP-behavior planning for cars," in *14th International IEEE Conference on Intelligent Transportation Systems*, Washington, DC, October 5–7 2011, pp. 1537–1542.
- [2] Y. Kuwata, J. Teo, G. Fiore, S. Karaman, E. Frazzoli, and J. P. How, "Real-time motion planning with applications to autonomous urban driving," *IEEE Transactions on Control Systems Technology*, vol. 17, no. 5, pp. 1105–1118, 2009.
- [3] S. Karaman and E. Frazzoli, "Sampling-based algorithms for optimal motion planning," *The International Journal of Robotics Research*, vol. 30, no. 7, pp. 846–894, 2011.
- [4] E. Velenis and P. Tsiotras, "Optimal velocity profile generation for given acceleration limits: theoretical analysis," in *Proceedings of the IEEE American Control Conference*, vol. 2, 2005, pp. 1478–1483.
- [5] C. You and P. Tsiotras, "High-speed cornering for autonomous off-road rally racing," *IEEE Transactions on Control Systems Technology*, pp. 1–17, 2019.
- [6] L. Jaillet, J. Cortés, and T. Siméon, "Sampling-based path planning on configuration-space costmaps," *IEEE Transactions on Robotics*, vol. 26, no. 4, pp. 635–646, 2010.
- [7] M. Garcia, A. Viguria, and A. Ollero, "Dynamic graph-search algorithm for global path planning in presence of hazardous weather," *Journal of Intelligent & Robotic Systems*, vol. 69, no. 1-4, pp. 285–295, 2013.
- [8] R. Cimurs, J. Hwang, and I. H. Suh, "Bézier curve-based smoothing for path planner with curvature constraint," in *IEEE International Conference on Robotic Computing*, Taichung, Taiwan, April 10–12 2017, pp. 241–248.
- [9] J.-w. Choi, R. Curry, and G. Elkaim, "Path planning based on Bézier curve for autonomous ground vehicles," in *World Congress on Engineering and Computer Science*, San Francisco, CA, October 22–24 2008, pp. 158–166.
- [10] J.-w. Choi, R. E. Curry, and G. H. Elkaim, "Continuous curvature path generation based on Bézier curves for autonomous vehicles," *International Journal of Applied Mathematics*, vol. 40, no. 2, pp. 91–101, 2010.
- [11] T. Shim, G. Adireddy, and H. Yuan, "Autonomous vehicle collision avoidance system using path planning and model-predictive-control-based active front steering and wheel torque control," *Proceedings of the Institution of Mechanical Engineers, Part D: Journal of automobile engineering*, vol. 226, no. 6, pp. 767–778, 2012.
- [12] J. Wang, M. A. Garratt, and S. G. Anavatti, "Real-time path planning algorithm for autonomous vehicles in unknown environments," *International Journal of Mechatronics and Automation*, vol. 6, no. 1, pp. 1–9, 2017.
- [13] W. Chee and M. Tomizuka, "Vehicle lane change maneuver in automated highway systems," Institute Of Transportation Studies, University of California, Berkeley, Tech. Rep. UCB-ITS-PRR-94-22, 1994.
- [14] T. Fraichard and A. Scheuer, "From Reeds and Shepp's to continuous-curvature paths," *IEEE Transactions on Robotics*, vol. 20, no. 6, pp. 1025–1035, 2004.
- [15] J. Chen, P. Zhao, T. Mei, and H. Liang, "Lane change path planning based on piecewise bezier curve for autonomous vehicle," in *Proceedings of 2013 IEEE International Conference on Vehicular Electronics and Safety*, 2013, pp. 17–22.
- [16] D. Korzeniowski and G. Ślaski, "Method of planning a reference trajectory of a single lane change manoeuvre with Bézier curve," in *IOP Conference Series: Materials Science and Engineering*, vol. 148, no. 1. IOP Publishing, 2016, p. 012012.
- [17] C. You, J. Lu, D. Filev, and P. Tsiotras, "Autonomous planning and control for intelligent vehicles in traffic," *IEEE Transactions on Intelligent Transportation Systems*, vol. 21, no. 6, pp. 2339–2349, 2020.
- [18] A. Kushleyev and M. Likhachev, "Time-bounded lattice for efficient planning in dynamic environments," in *IEEE International Conference on Robotics and Automation*, Kobe, Japan, 2009, pp. 1662–1668.
- [19] M. Pivtoraiko, R. A. Knepper, and A. Kelly, "Differentially constrained mobile robot motion planning in state lattices," *Journal of Field Robotics*, vol. 26, no. 3, pp. 308–333, 2009.
- [20] J. Ziegler and C. Stiller, "Spatiotemporal state lattices for fast trajectory planning in dynamic on-road driving scenarios," in *IEEE/RSJ International Conference on Intelligent Robots and Systems*, 2009, pp. 1879–1884.
- [21] M. McNaughton, C. Urmson, J. M. Dolan, and J.-W. Lee, "Motion planning for autonomous driving with a conformal spatiotemporal lattice," in *IEEE International Conference on Robotics and Automation*, Shanghai, China, 2011, pp. 4889–4895.
- [22] R. Chandra, Y. Selvaraj, M. Brännström, R. Kianfar, and N. Murgovski, "Safe autonomous lane changes in dense traffic," in *IEEE 20th International Conference on Intelligent Transportation Systems*, 2017, pp. 1–6.
- [23] M. Obayashi and G. Takano, "Real-time autonomous car motion planning using nmpc with approximated problem considering traffic environment," *IFAC-PapersOnLine*, vol. 51, no. 20, pp. 279–286, 2018.
- [24] J. Chen, W. Zhan, and M. Tomizuka, "Autonomous driving motion planning with constrained iterative LQR," *IEEE Transactions on Intelligent Vehicles*, vol. 4, no. 2, pp. 244–254, 2019.
- [25] Y. Zhao, Y. Wang, M. Zhou, and J. Wu, "Energy-optimal collision-free motion planning for multi-axis motion systems: An alternating quadratic programming approach," *IEEE Transactions on Automation Science and Engineering*, vol. 16, no. 1, pp. 327–338, 2018.
- [26] Y. Pan, Q. Lin, H. Shah, and J. M. Dolan, "Safe planning for self-driving via adaptive constrained ILQR," *arXiv preprint arXiv:2003.02757*, 2020.
- [27] P. E. Hart, N. J. Nilsson, and B. Raphael, "A formal basis for the heuristic determination of minimum cost paths," *IEEE transactions on Systems Science and Cybernetics*, vol. 4, no. 2, pp. 100–107, 1968.
- [28] S. Koenig and M. Likhachev, "D* lite," *Aaai/iaai*, vol. 15, 2002.
- [29] D. González, J. Pérez, V. Milanés, and F. Nashashibi, "A review of motion planning techniques for automated vehicles," *IEEE Transactions on Intelligent Transportation Systems*, vol. 17, no. 4, pp. 1135–1145, 2015.
- [30] D. Q. Mayne, "Differential dynamic programming—a unified approach to the optimization of dynamic systems," in *Control and Dynamic Systems*. Elsevier, 1973, vol. 10, pp. 179–254.
- [31] J. Chen, W. Zhan, and M. Tomizuka, "Constrained iterative lqr for on-road autonomous driving motion planning," in *IEEE 20th International Conference on Intelligent Transportation Systems*, 2017, pp. 1–7.
- [32] P. E. Gill, W. Murray, and M. A. Saunders, "SNOPT: An SQP algorithm for large-scale constrained optimization," *SIAM review*, vol. 47, no. 1, pp. 99–131, 2005.
- [33] L. T. Biegler and V. M. Zavala, "Large-scale nonlinear programming using IPOPT: An integrating framework for enterprise-wide dynamic optimization," *Computers & Chemical Engineering*, vol. 33, no. 3, pp. 575–582, 2009.
- [34] E. Todorov and W. Li, "A generalized iterative LQG method for locally-optimal feedback control of constrained nonlinear stochastic systems," in *Proceedings of the IEEE American Control Conference*, 2005, pp. 300–306.
- [35] A. Philipp and D. Goehring, "Analytic collision risk calculation for autonomous vehicle navigation," in *International Conference on Robotics and Automation*, 2019, pp. 1744–1750.
- [36] A. Gessner, O. Kanjilal, and P. Hennig, "Integrals over Gaussians under linear domain constraints," in *International Conference on Artificial Intelligence and Statistics*. PMLR, 2020, pp. 2764–2774.
- [37] L.-z. Liao and C. A. Shoemaker, "Advantages of differential dynamic programming over Newton's method for discrete-time optimal control problems," Cornell University, Tech. Rep., 1992.
- [38] M. Treiber, A. Hennecke, and D. Helbing, "Congested traffic states in empirical observations and microscopic simulations," *Physical review E*, vol. 62, no. 2, p. 1805, 2000.



Changxi You is a senior researcher in Autonomous Driving Laboratory at Tencent Technology Company. He received his B.S. and M.S. degrees from the Department of Automotive Engineering, Tsinghua University of China, and a second M.S. degree from the Department of Automotive Engineering, RWTH-Aachen University of Germany. He received his Ph.D. degree under the supervision of Prof. Panagiotis Tsiotras from the School of Aerospace Engineering, Georgia Institute of Technology. His current research interests are in motion planning & control in congested traffic, collision avoidance in uncertain environment, and intelligent coordination and control for large-scale traffic signals.